ILD benchmark: tau tau at 500 GeV

Daniel Jeans, Keita Yumino

April 26, 2019

Abstract

Analysis of polarimetry in the process $ee \to \tau\tau$ at 500 GeV for detector benchmarking.

1 Introduction

Tau pair production at high centre-of-mass. The polarisation of tau lepton is reconstructable thanks to its relatively short lifetime and "clean" decays. The distribution of tau decay products reflects the direction of its spin.

We study the selection of such events, how well the different tau decay modes can be identified, and how their spin can be reconstructed. We compare the performance of the two ILD detector models (Large IDR-L and Small IDR-S).

2 What we need to measure

The tau decay gives us sensitivity to its spin, and therefore to the left and right handed couplings of whatever intermediate particle produced them. In the $ee \to \tau\tau$ process, we plot the scattering angle and tau-tau invariant mass in Fig.1. These are shown at MC level, separately for samples with (100%) eLpR and eRpL beam polarisations.

We also plot the "exact" polarimeters in the case of $\tau^\pm \to \pi^\pm\nu$ and $\tau^\pm \to \pi^\pm\pi^0\nu$ decays. The polarimeter vectors are defined in the tau rest frames as follows: for $\tau^\pm \to \pi^\pm\nu$, it is the direction of the neutrino momentum, while for $\tau^\pm \to \pi^\pm\pi^0\nu$ it is the direction of the vector $\mathbf{P} = 2(\mathbf{q}\cdot\mathbf{p}_\nu)\mathbf{q} - m_q^2\mathbf{p}_\nu$, where $\mathbf{q} = \mathbf{p}_{\pi^\pm} - \mathbf{p}_{\pi^0}$, and $\mathbf{p}_\nu, \mathbf{p}_{\pi^\pm}, \mathbf{p}_{\pi^0}$ are respectively the 3-momenta of the neutrino, charged and neutral pions. To distinguish taus of different helicity, we look at the cosine of the angle this polarimeter vector makes to the tau flight direction.

It proves difficult to reconstruct this optimal polarimeter in the case of rho decays in the di-tau event topology at these high energies (although this may be possible with further study). For the time being, we therefore adopt an approach which makes use of only the visible 4-vectors of the charged and neutral pions produced in rho decay, integrating over possible neutrino configurations, as described in [1], the results of which are reproduced in appendix A. The resulting "approximate" polarimeters are compared with the "exact" ones in figures 2 and 3 respectively for $\tau^\pm \to \pi^\pm\nu$ and $\tau^\pm \to \pi^\pm\pi^0\nu$ decays.

The aim of this analysis is essentially to see how well we can reconstruct these distributions in the large and small ILD models.

3 Event selection

It is the semi-leptonic tau decays (in which the tau decays to a single neutrino plus hadrons) which are most sensitive to tau polarisation (fully leptonic modes suffer from the presence of 2 neutrinos per tau decay). We therefore emphasise hadronic decays, in particular $\tau^\pm \to \pi^\pm\nu$ (the cleanest hadronic decay) and $\tau^\pm \to \pi^\pm\pi^0\nu$ (which has the largest decay branching ratio, accounting for around 26% of tau decays). These two decay modes both allow full extraction of polarisation information. We concentrate our efforts on events in which the tau pair invariant mass is close to the nominal collision energy of 500 GeV.

From the detector point of view, the identification and measurement of the charged hadron is rather easy. The most sensitive aspect is probably the reconstruction and measurement of the π^0 decay products in the highly boosted tau decays.

We first apply a simple preselection, requiring that between 2 and 12 charged PFOs have been reconstructed, to remove the majority of events with hadronic jets. We then look for two seed directions around which to build tau jet candidates. We identify the highest momentum charged PFO in the event ("first seed"). Once this has been found, we look for the next highest momentum charged PFO which is separated from the first seed by at least $\pi/2$ in the $x-y$ plane ($\delta\phi$). This selection makes use of the property that the two taus in

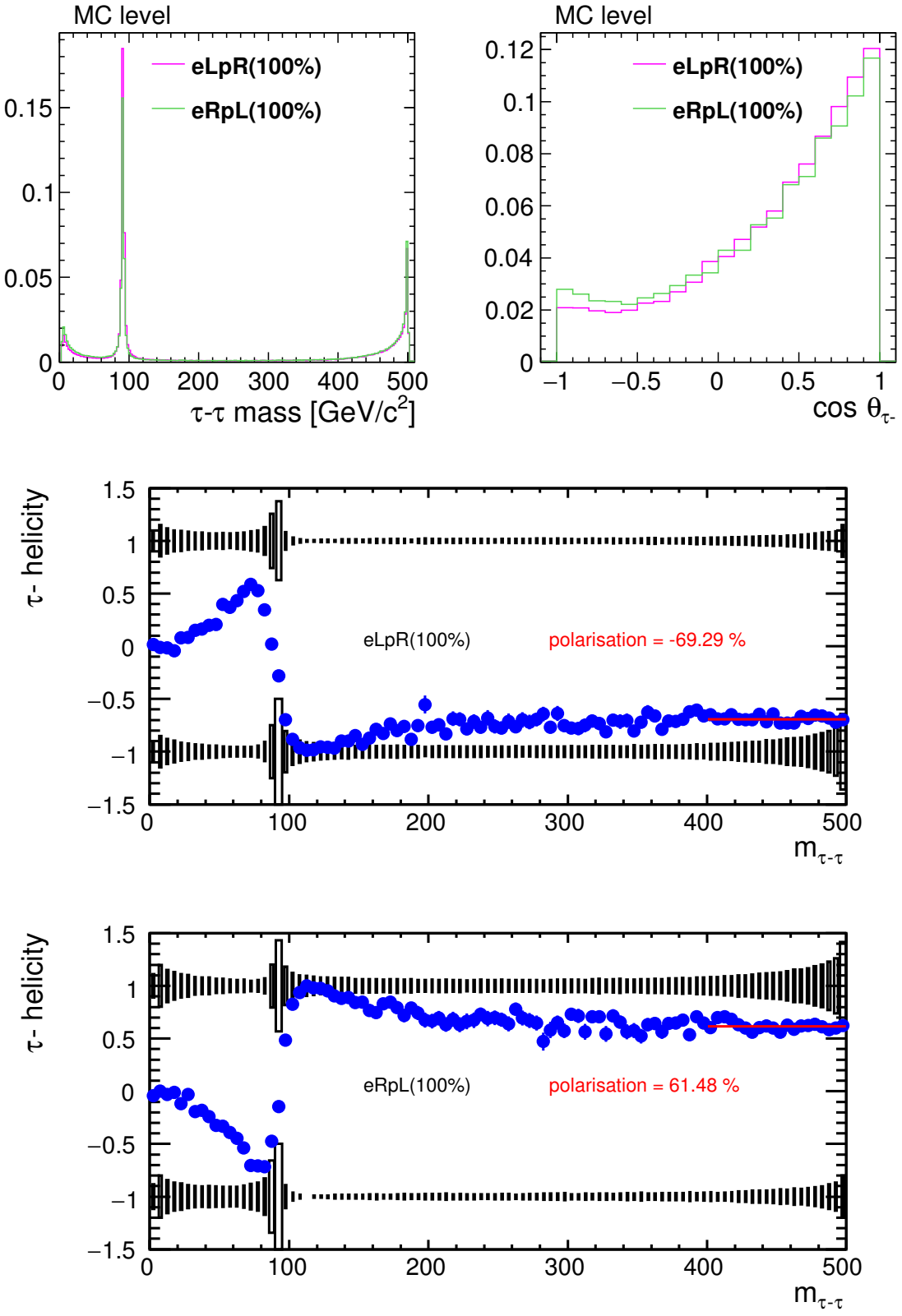

Figure 1: MC distributions: the tau-tau invariant mass $m_{\tau\tau}$, $\cos\theta_{\tau-}$ for events with $m_{\tau\tau} > 480$ GeV, and the tau polarisation as a function of $m_{\tau\tau}$.

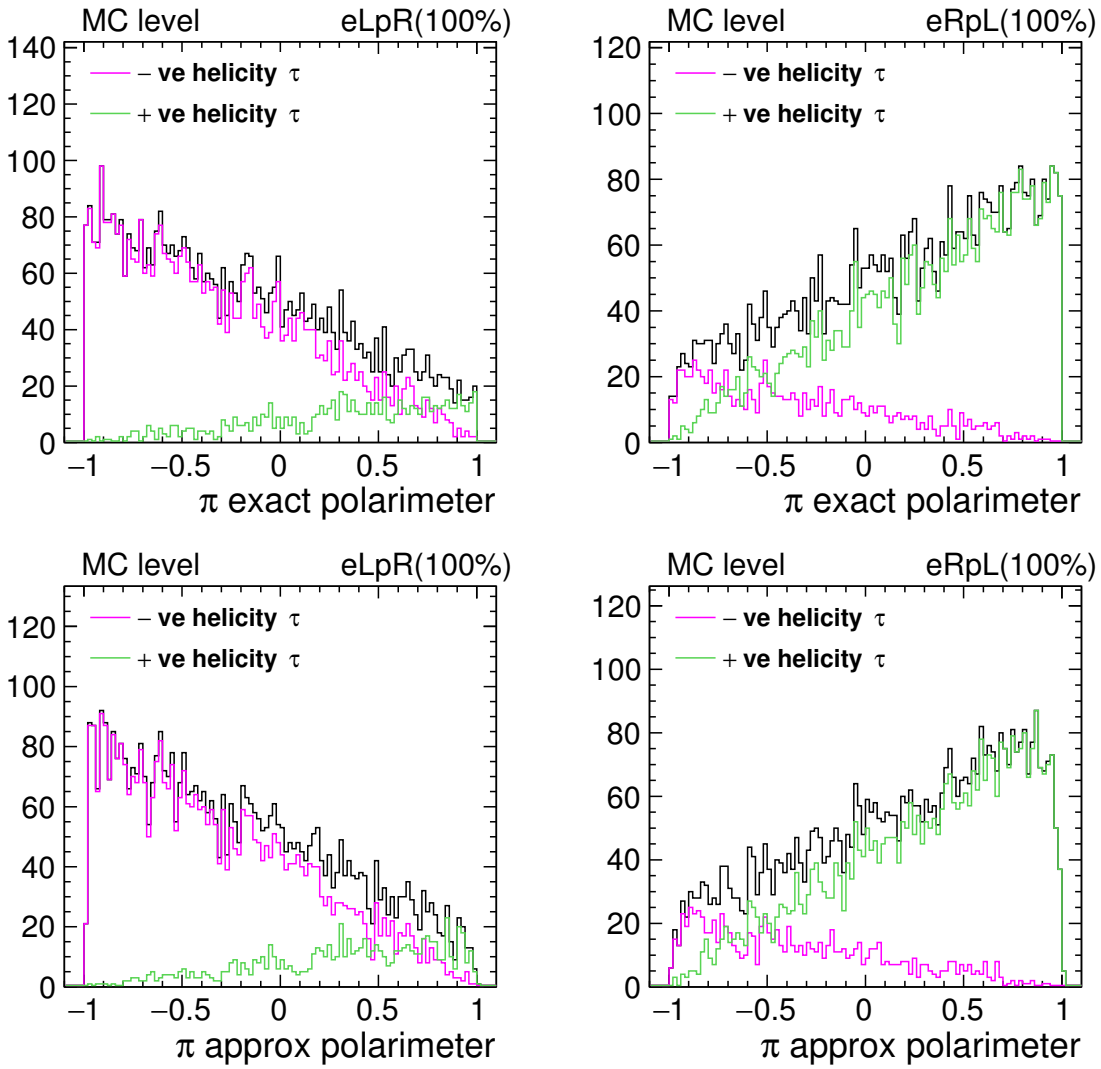

Figure 2: MC distributions. Pi polarimeters, for events with $m_{\tau\tau} > 480$ GeV.

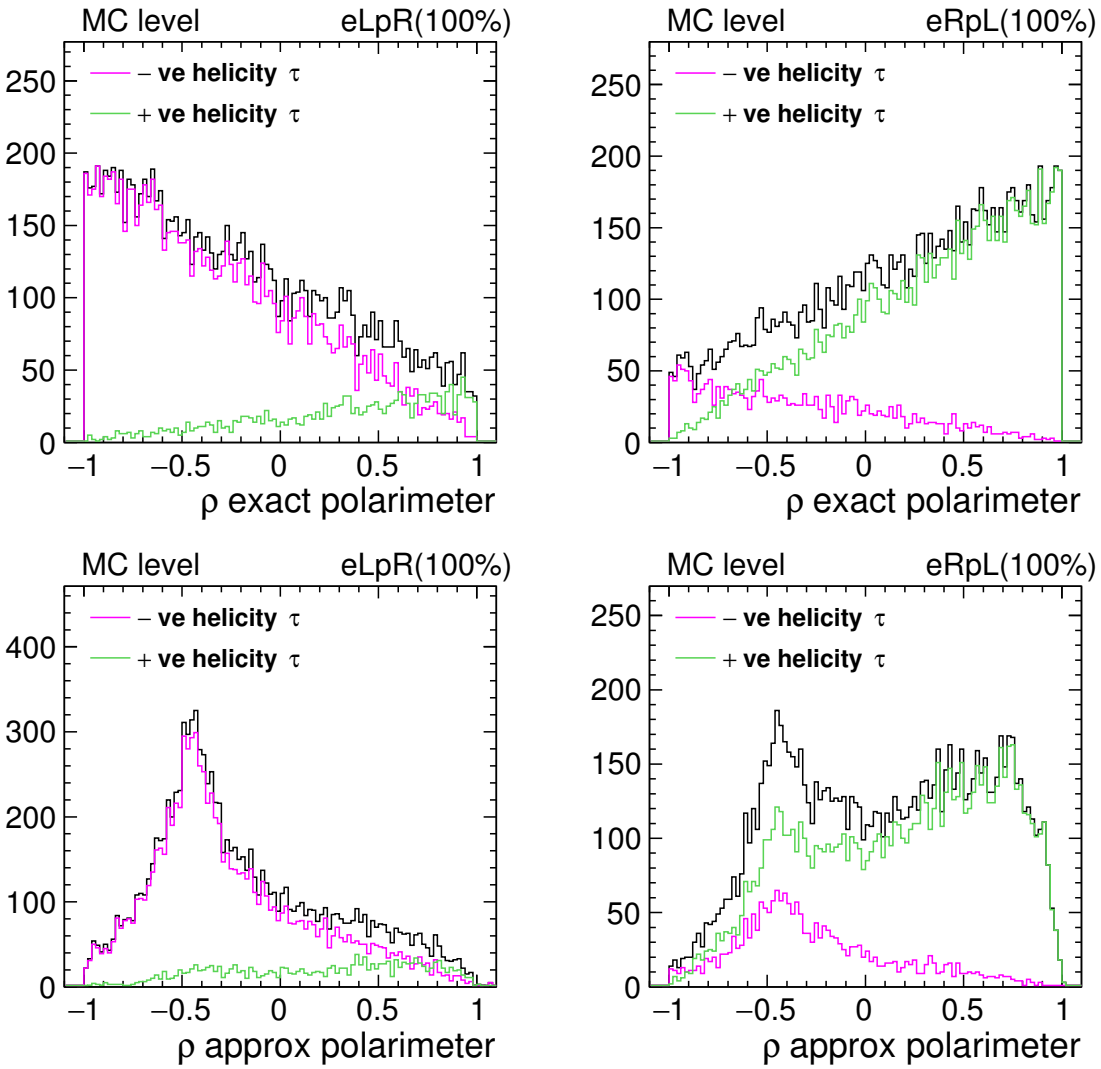

Figure 3: MC distributions. Rho polarimeters for events with $m_{\tau\tau} > 480$ GeV.

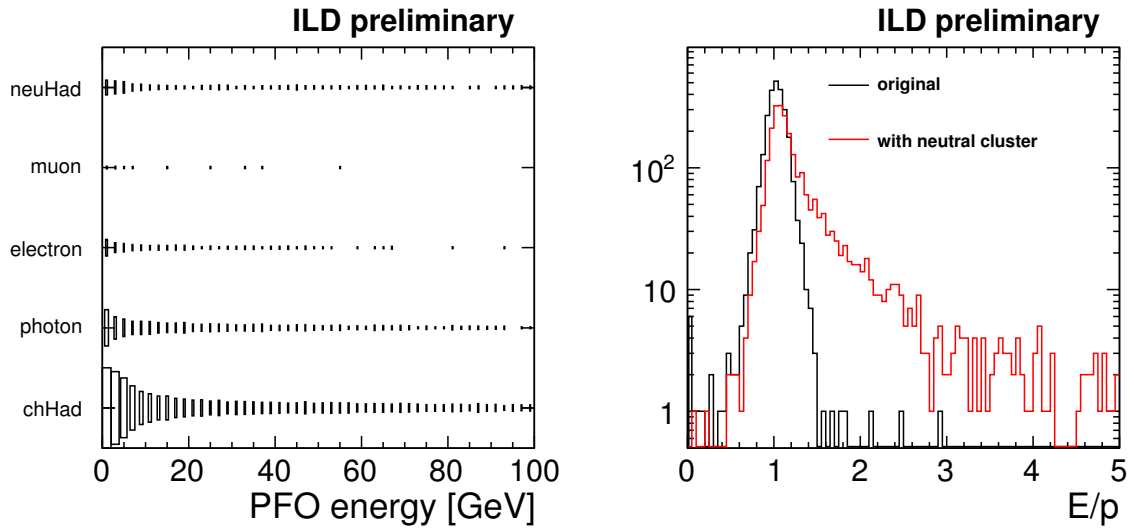

Figure 4: Left: the nature of the MC particle which created PFOs flagged as neutral hadrons, as a function of PFO energy. Right: Events with one charged hadron and one one neutral hadron PFO: the E/p of the charged hadron before and after adding the neutral hadron cluster energy to it.

signal events are emitted back-to-back in the $x-y$ plane in the case of collinear (or no) ISR. If no second seed is found, the event is rejected.

We then look in narrow cones (opening angle 0.1 rad) around these two seed directions. PFOs within these cones are associated to tau jet candidates. The cluster associated to each seed particle is modeled as an ellipsoid, whose eigenvalues (the lengths of its axes) are used in the selection. We then apply the following selection:

- Energy of the second seed less than 200 GeV. [to remove di-lepton events.]
- Sum of the energy (p_T) of particles lying outside the two cones less than 40 (20) GeV. [remove hadronic events.]
- acoplanarity between candidate jet directions less than 0.05 rad. [remove fully leptonic WW events]
- acolinearity between candidate jet directions less than 0.075 rad. [remove Z return events.]
- No photon-like PFO (as tagged by PandoraPFA) with energy larger than 10 GeV lying outside the two cones. [remove events with seen ISR]
- No isolated leptons identified by the IsolatedLeptonTaggingProcessor. [remove dilepton events, fully leptonic tau decays]
- The smallest and largest eigenvalues of the shower ellipsoid must respectively lie in the range $10^{1.0}$ and $10^{3.6}$ mm, and $10^{1.6}$ and $10^{4.0}$ mm.

We then look in more detail at the two jet cones. We observe that neutral hadrons are often reconstructed within the cones. This is almost always the result of fragmentation of the calorimetric shower induced by a charged hadron. The number of long-lived neutral hadrons produced in tau decays is rather small, so we remove such neutral hadron PFOs from the event. In Fig. 4, we look at the parent particle of those clusters flagged as neutral hadrons: the majority are due to fragmentation of the charged hadron. In the same figure we compare the E/p of the original charged hadron PFO, and what we obtain when the neutral hadron cluster energy is added: the E/p distribution is degraded when the neutral hadron is added: this helps understand why the reconstruction algorithm chooses to split off part of the hadronic shower into a distinct PFO.

In addition, if the total charge of the jet is zero, we remove the charged particle furthest from the jet's initial seed direction. After removing these PFOs from consideration, we calculate the invariant mass of the jet. We require that this mass is less than 1.77 GeV, and also that the produce of the two jets' charges is -1.

Fig. 6 shows the number of photon-like PFOs identified within the jet cone, in the case that the cone is matched (in angle) to various tau decays at the MC level. In the case of ρ decays, in around half of tau jets only a single photon cluster is reconstructed. Fig 5 shows the reasons that only a single photon cluster is sometimes found in rho decays:

- "converted": at least one photon converted in the tracking region (and was not identified as such in the event reconstruction);

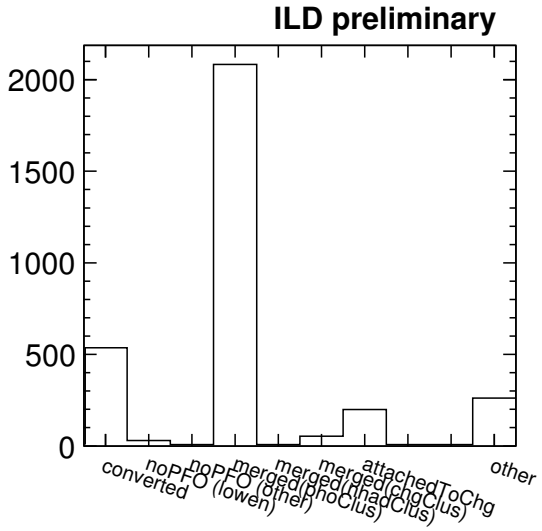

Figure 5: Reason for which only a single photon PFO was found in $\tau \to \rho$ decays. (see text for details.)

final state	$ee \to \tau\tau$			2f	4f
	SIGNAL		OTHER		
	efficiency [%]	expected events/1000			
original	100.0	221.8	5214.0	36801.2	51915.0
preselected	88.5	196.3	4513.7	7560.3	16259.6
two seeds	88.2	195.6	4277.2	7217.0	14364.8
out-of-cone activity	83.8	185.9	2441.4	1728.5	5880.3
acolinearity	82.1	182.2	1848.6	1140.5	708.2
acoplanarity	76.5	169.7	343.2	4.6	121.4
ISR veto	74.6	165.5	329.1	4.4	115.9
isolated lepton veto	74.0	164.2	235.6	3.2	28.8
seed cluster shape	65.7	145.8	25.1	2.5	2.2
candidate jet mass	56.3	124.8	17.2	0.3	1.4
jets' charge	54.6	121.0	16.2	0.3	1.3

Table 1: Selection efficiencies and expected event numbers at different stages of the selection (see text for details). Large detector IDR-L, 1.8ab^{-1} in the eLpR polarisation. SIGNAL refers to $ee \to \tau\tau$ events with $\tau\tau$ invariant mass greater than 480 GeV, and in which both τs decay hadronically.

- "noPFO (lowen)": no PFO associated with the photon was found (and at least one photon energy < 300 MeV);
- "noPFO (other)": no PFO associated with the photon was found (and both photon energies > 300 MeV);
- "merged (phoClus)": the two photons were attached to the same photon PFO;
- "merged (nhadClus)": the two photons were attached to the same neutral hadron PFO;
- "merged (chgClus)": the two photons were attached to the same charged hadron PFO;
- "attachedToChg": one photon was attached to a charged hadron PFO.

The most common reason for mis-counting the number of photons is that the two photons have been merged into a single photon-like cluster. To investigate whether the shape of the resulting cluster can be used to identify such "merged photon" clusters, we show in fig. reffig:clustermerge the smaller two eigenvalues of the ellipsoid which describes the shape of the calorimetric cluster, for clusters which originate in a single photon, and those which are the result of a di-photon merger. There is no clear difference between the two polulations, apart fram rather different distributions of the clusters' energy.

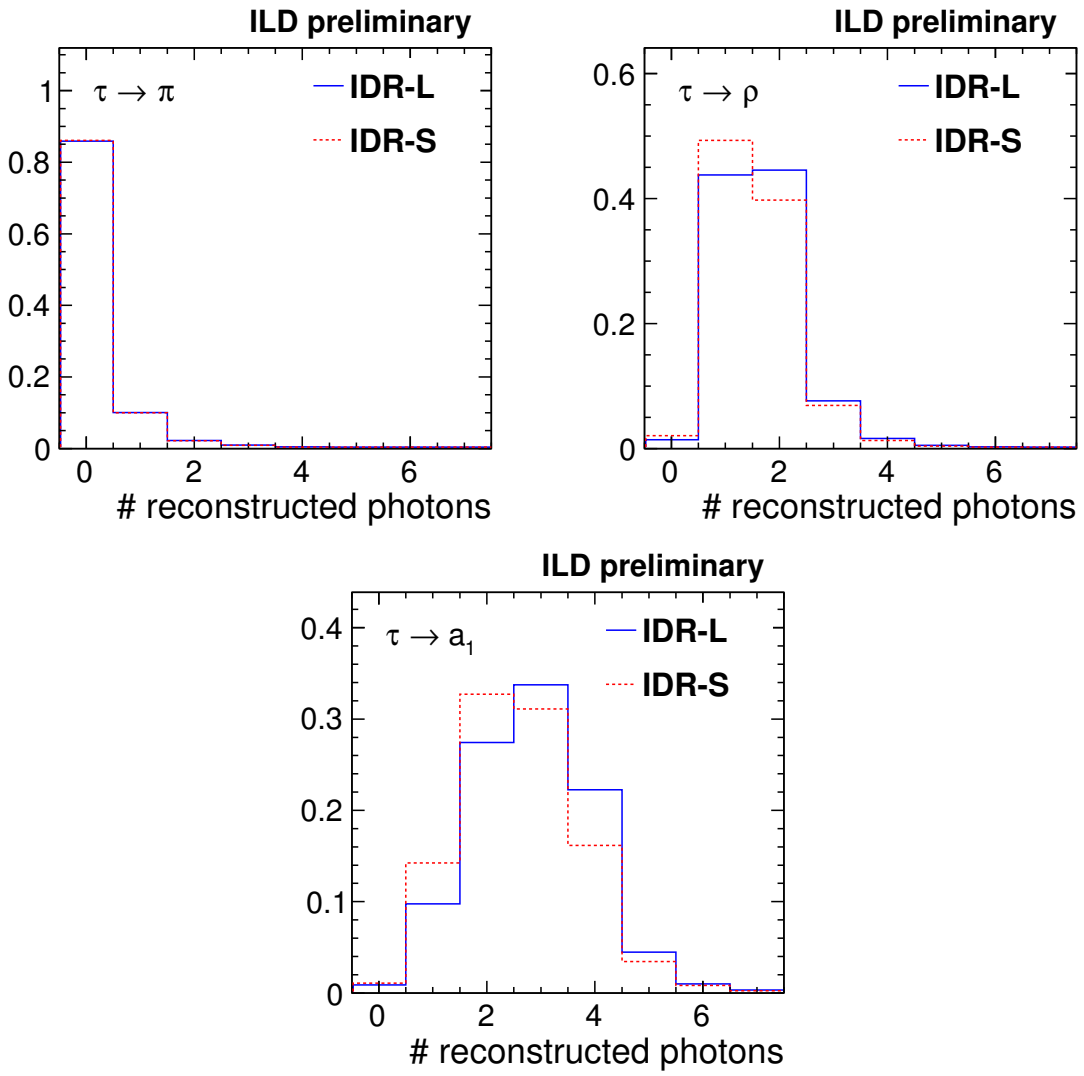

Figure 6: Signal-only comparisons after general event selection: the number of reco photons in candidate jets matched to taus decaying in the single pion, rho, and single-prong a1 modes. The expected number of photons produced in these decays is respectively 0, 2, and 4 in these decay models.

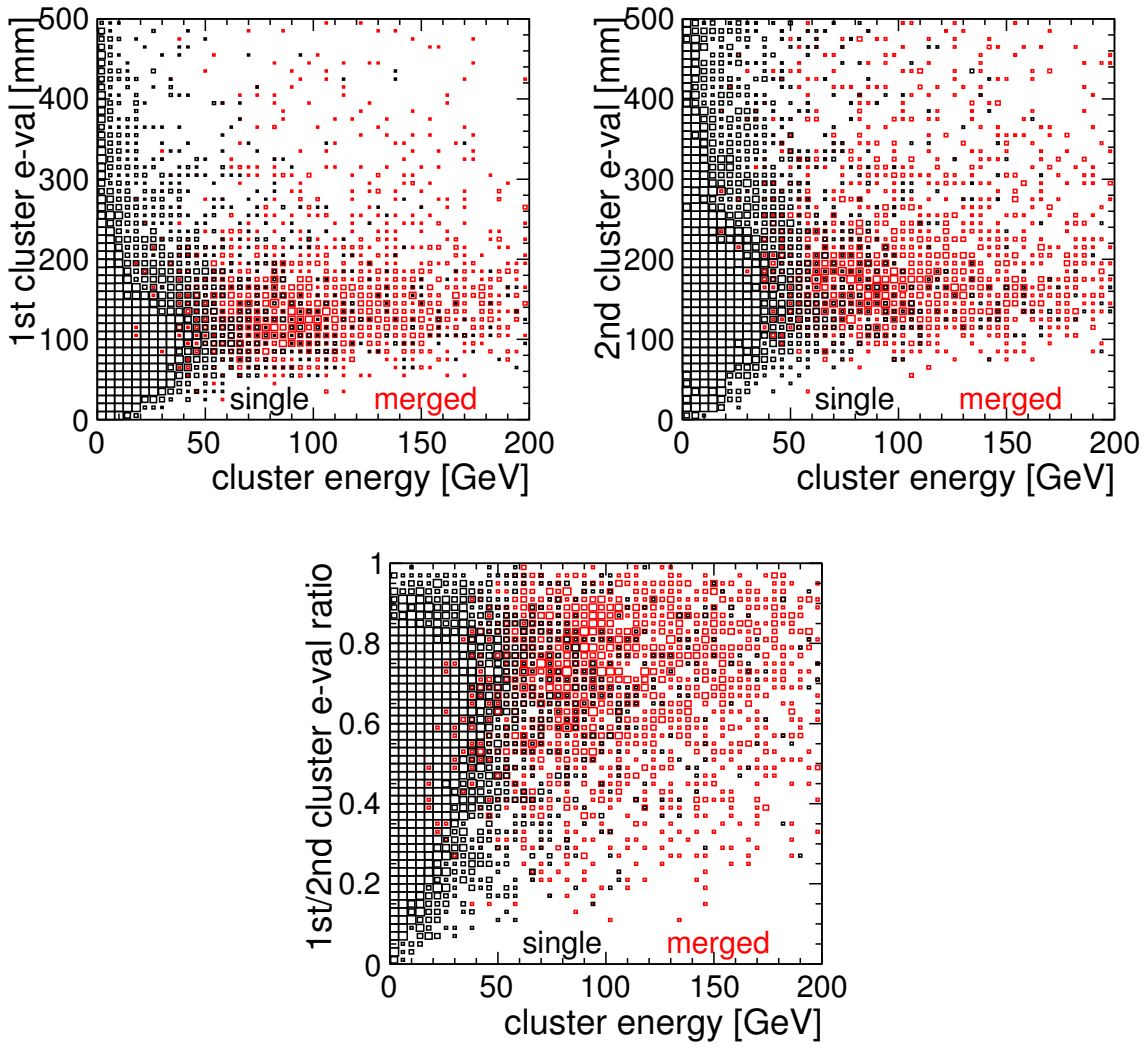

Figure 7: First (smallest) and second eigenvalues and their ratio, of the ellipsoid fitted to photon-like clusters found in $\tau \to \rho$ decay jets. The contribution from clusters resulting from the merger of two clusters is shown in red, and single-photon clusters in black.

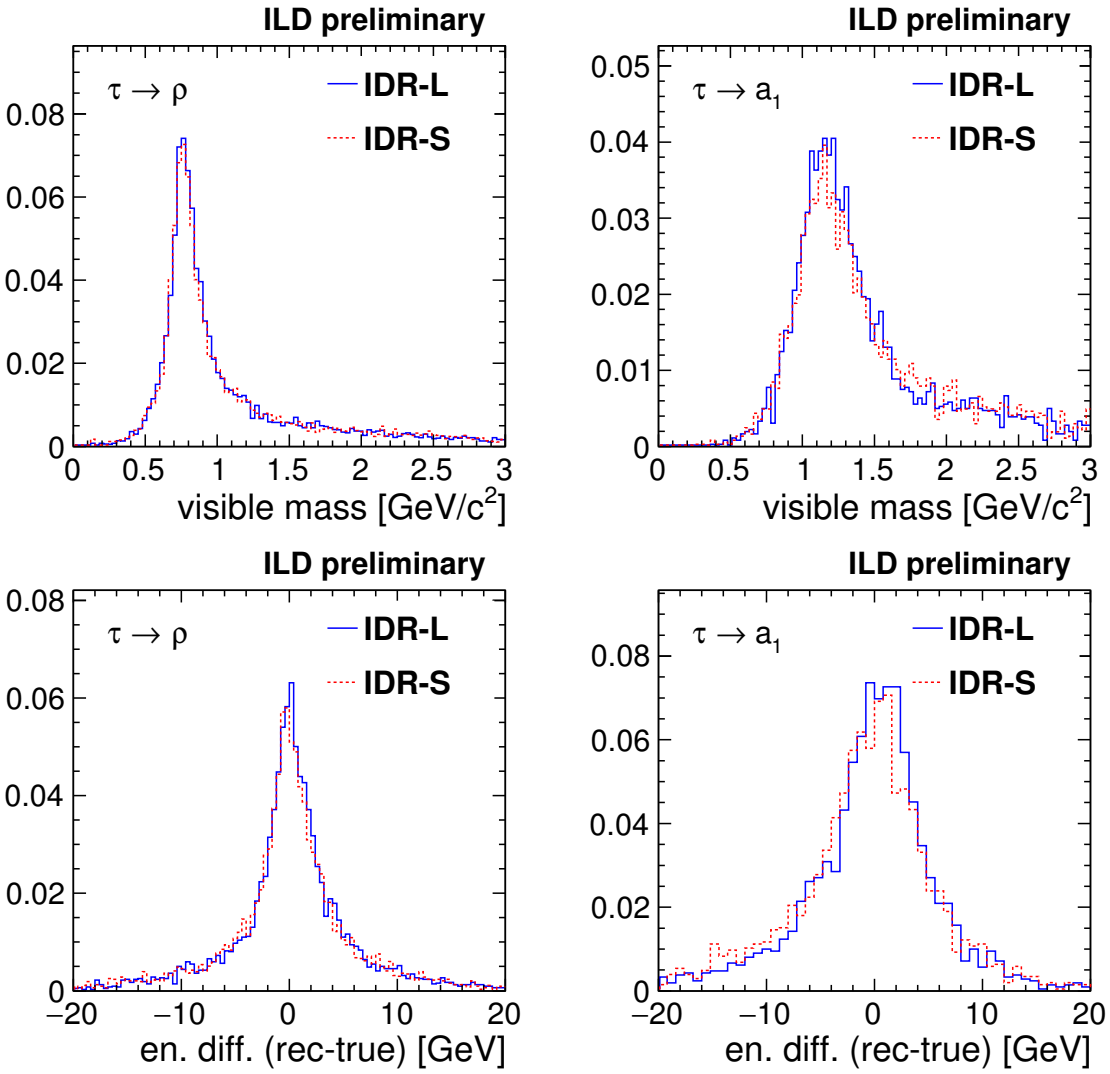

Figure 8: Signal-only comparisons after general event selection. visible invariant mass and the difference between the true and reconstructed visible energy.

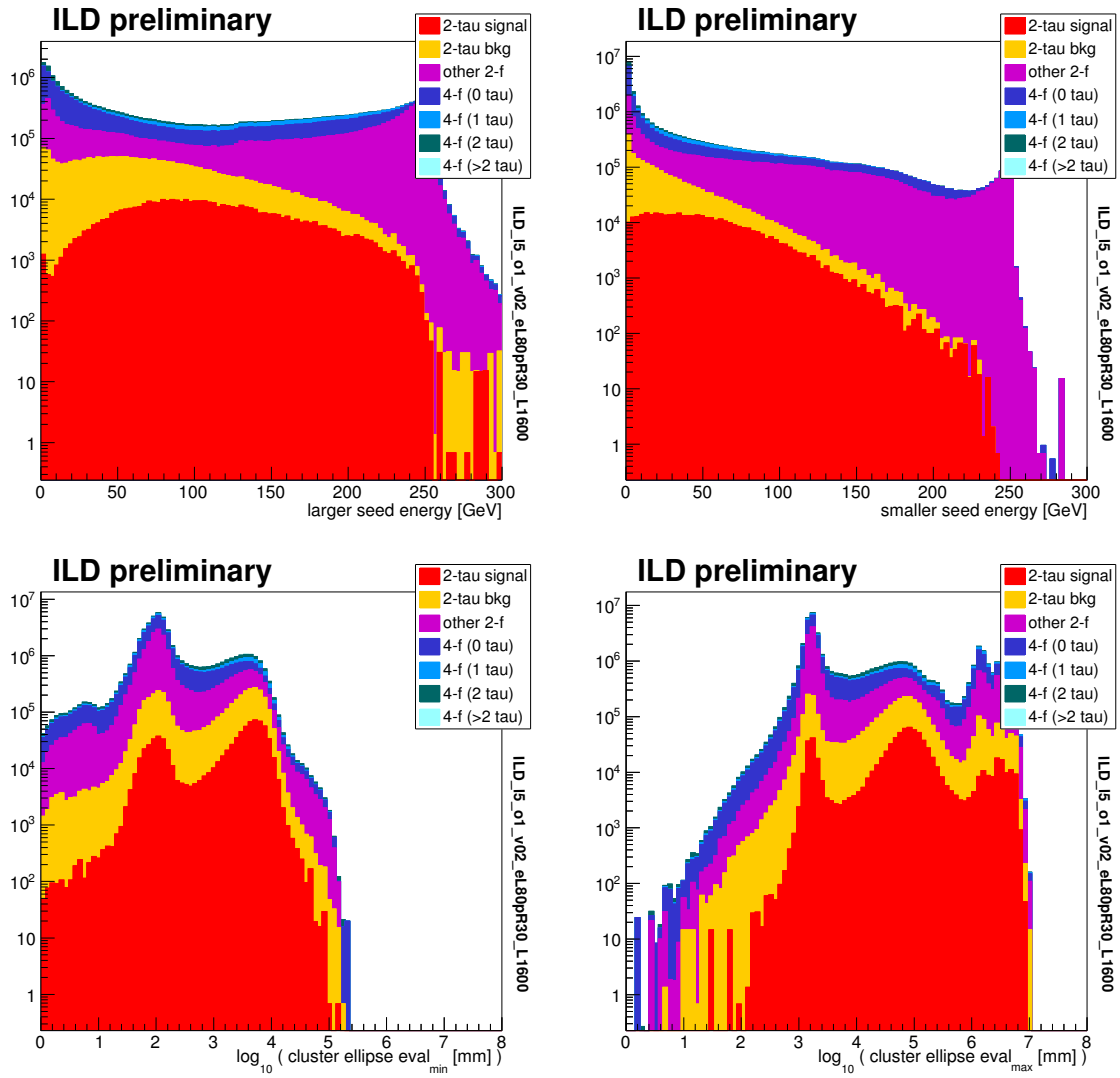

Figure 9: Distributions after preselection. The larger and smaller of the seed PFOs' energies, and the smaller and larger of the seeds' associated calorimeter cluster shape eigenvalues.

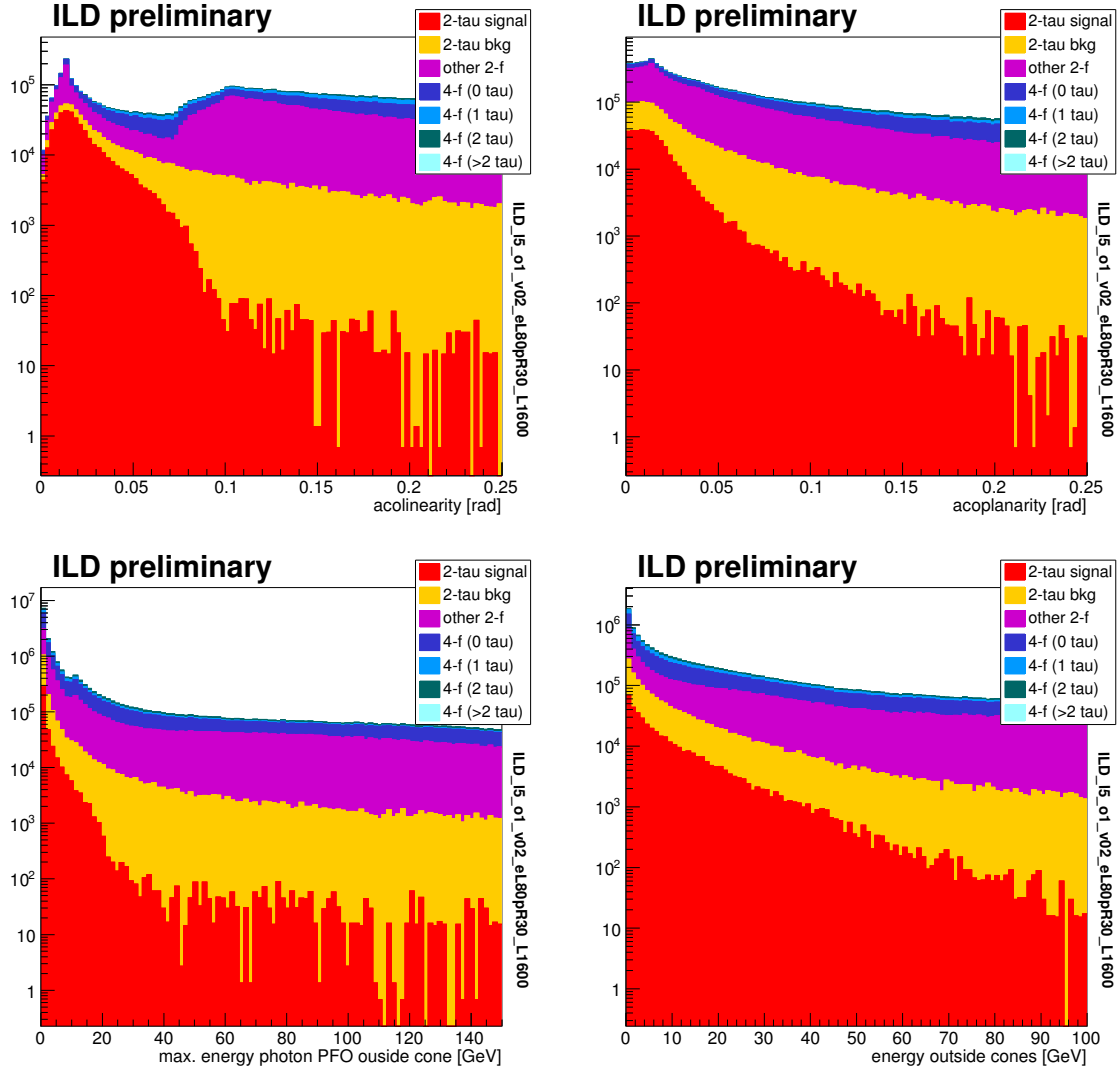

Figure 10: Distributions after preselection. Acolinearity and acoplanarity of the two candidate jets, the energy of most energetic photon PFO found outside the two jet cones, and the sum of the energy of all particles outside the cones.

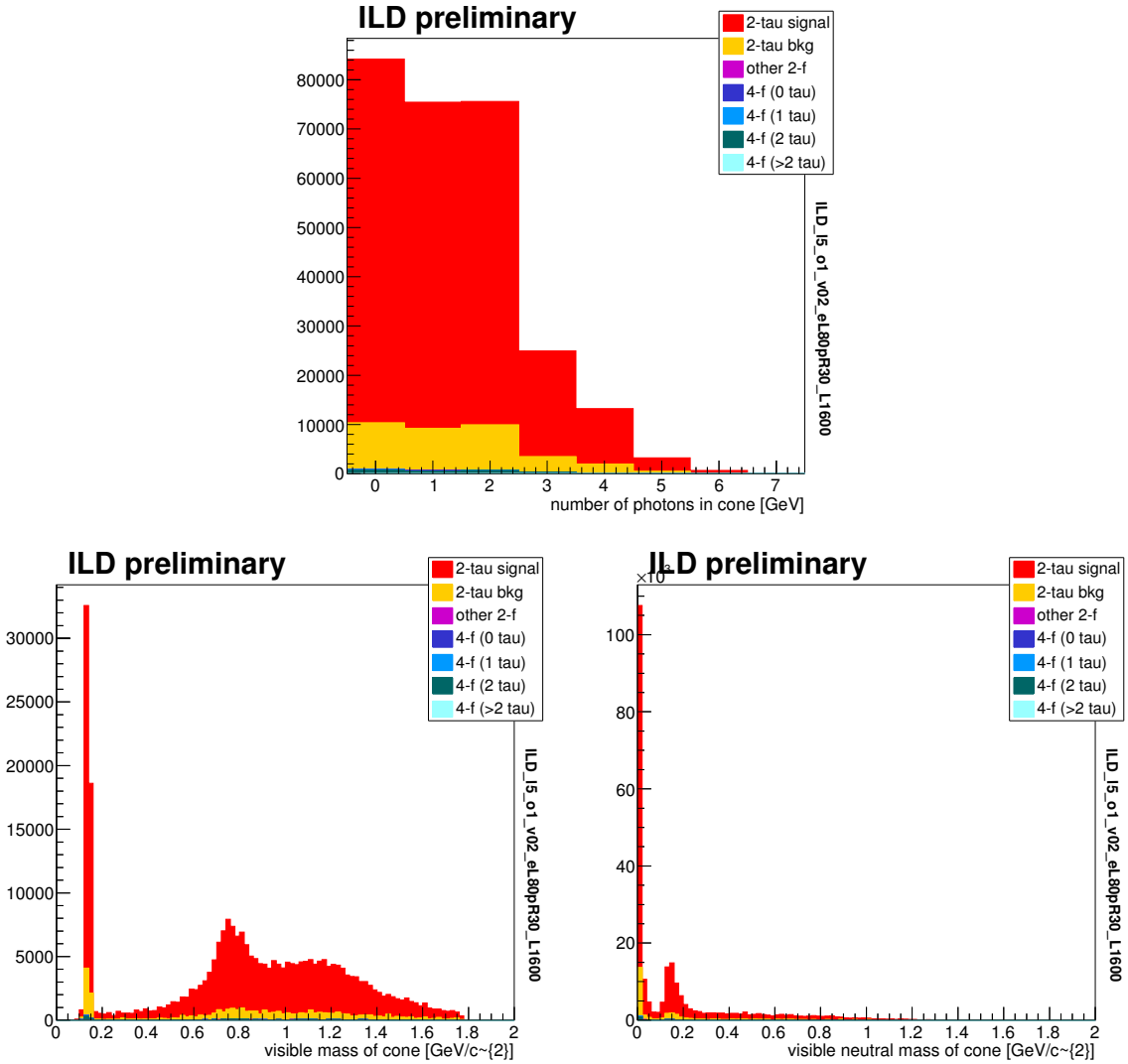

Figure 11: Distributions after preselection. The number of photon PFOs found per candidate jet, and the invariant mass of all (neutral) PFOs inside the jet.

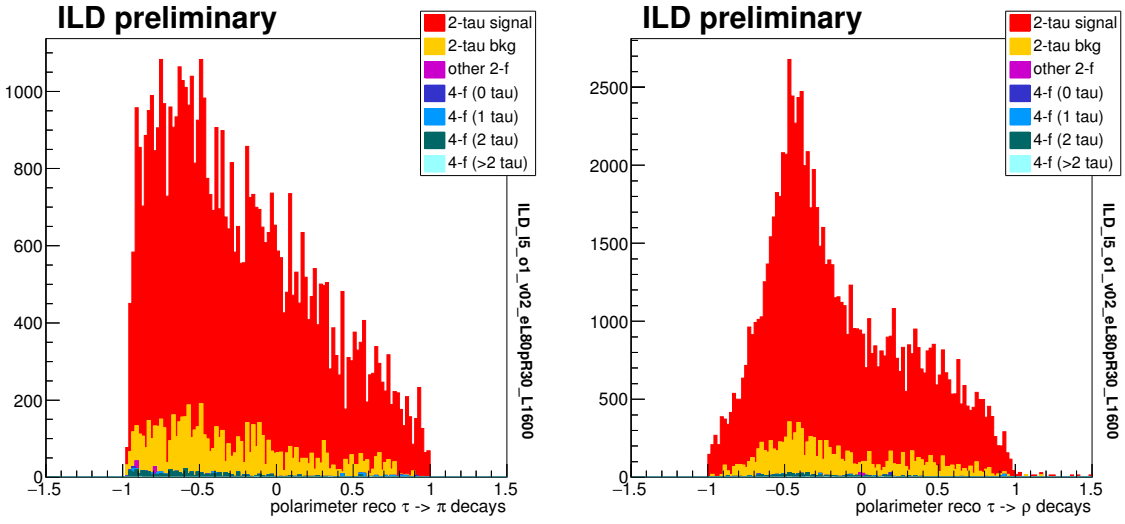

Figure 12: Distributions after preselection. Reconstructed polarimeters in jets identified as $\tau \to \pi, \rho$ decays.

ILD_l5_o1_v02	MC-pi	MC-rho	MC-a1p	MC-other	purity
SELECTED AS PI	89.62 ± 0.40	1.88 ± 0.12	0.81 ± 0.14	9.30 ± 0.30	82.50 ± 0.47
SELECTED AS RHO	6.52 ± 0.32	76.51 ± 0.37	12.77 ± 0.51	5.76 ± 0.24	87.08 ± 0.32
SELECTED AS A1P	2.28 ± 0.19	13.24 ± 0.30	66.40 ± 0.72	6.82 ± 0.26	53.72 ± 0.68
ILD_s5_o1_v02	MC-pi	MC-rho	MC-a1p	MC-other	purity
SELECTED AS PI	88.85 ± 0.41	3.09 ± 0.15	1.05 ± 0.16	9.84 ± 0.31	79.78 ± 0.49
SELECTED AS RHO	7.55 ± 0.34	74.89 ± 0.39	16.89 ± 0.58	5.88 ± 0.25	84.82 ± 0.34
SELECTED AS A1P	2.16 ± 0.19	14.07 ± 0.31	60.30 ± 0.75	6.33 ± 0.25	50.53 ± 0.71

Table 2: Selected 1-prong tau candidates in signal events: decay mode identification efficiency in large and small models (unpolarised sample), and the purity considering only backgrounds from the signal process.

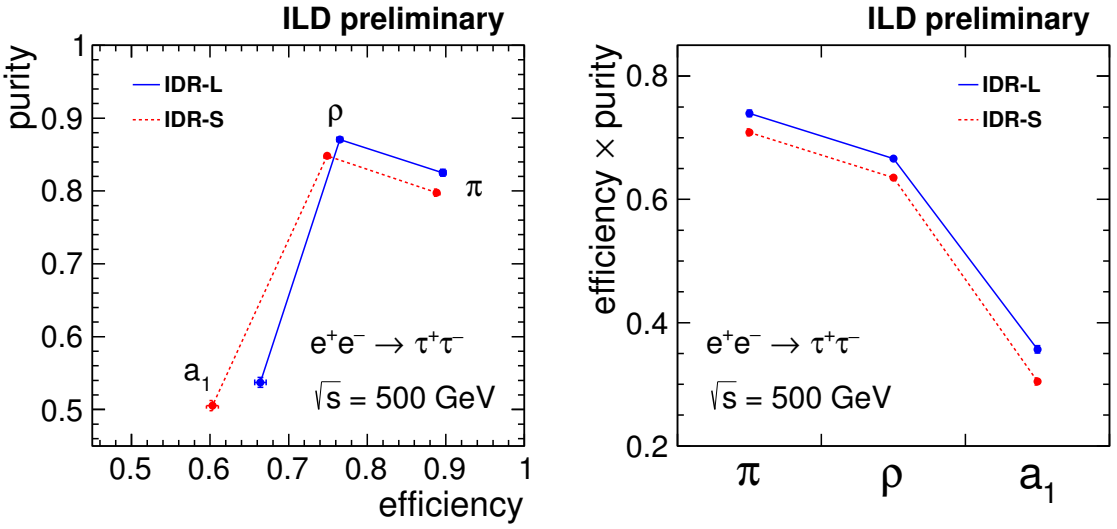

Figure 13: Separation of single prong tau decay modes: the efficiency and purity (left) and their product (right) of the decay mode selection described in the text. The purity definition includes only other high mass di-tau events as background.

4 Tau decay mode selection

To decide whether a jet originates from $\tau^{\pm} \to \pi^{\pm}\nu$ or $\tau^{\pm} \to \pi^{\pm}\pi^{0}\nu$, we first require that it contains a single charged PFO. A cut-based selection is based on 3 observables of particles in the trimmed candidate jet:

- number of identified photon PFOs,
- total invariant mass of all visible particles, and
- total invariant mass of all neutral visible particles.

The same selection criteria are used in both detectors models. The performance of this identification in both models is shown in table 2 and summarised graphically in Fig. 13.

As shown in both the table and the plot, the performance of the large detector model is somewhat better than the small one, with slightly better efficiency and/or purity when selecting these three decay modes.

The efficiency to select events and correctly identify tau decay modes may have some dependence on the helicity of the taus involved. Such a dependence might introduce a bias on the extraction of the tau polarisation, if this is not corrected for. The dependence on the selection and reconstruction efficiency on the exact polarimeters is shown in figure 14. Some dependence is seen, most notably around -1 for $\pi^{\pm}$ decays: this can be understood since it corresponds to a very soft charged pion.

5 Polarimeter estimation

We here discuss how to extract polarisation information from measurements of the tau decay products.

In the present analysis, we adopt an approach which makes use of only the visible 4-vectors of the charged (and potentially neutral) pions produced in the tau decay, as described in [1]. We use just the pi and rho decays. In the case of the pi, we use just the energy of the pion, while rho decays make use of a much more complicated

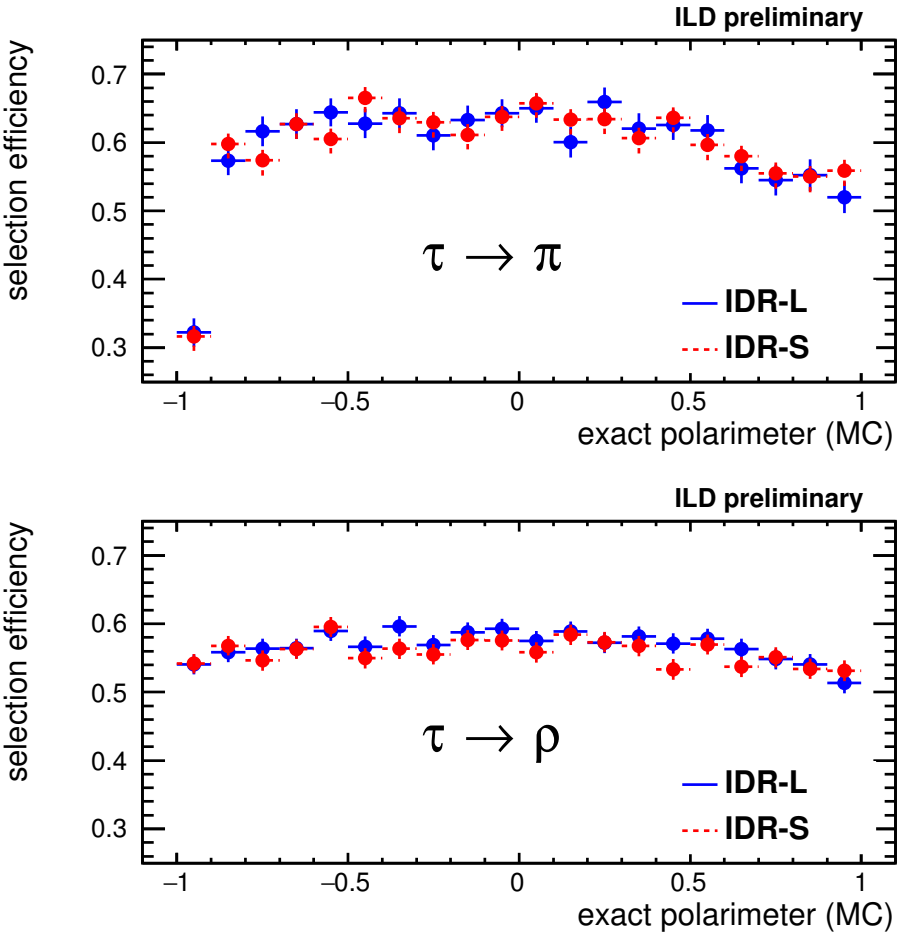

Figure 14: Selection and reconstruction efficiency for taus in the two considered decay modes, as a function of the true value of the polarimeter.

function of the measured momenta, as described in the above reference and reproduced in an appendix to this note.

In fig 15 we show the signal-only reconstructed polarimeters in the two detector models and for 100% polarisation scenarios, and their difference to the MC truth, for tau jets whose decay has been correctly identified, in selected events. The shapes of the distributions clearly show differences, and some small differences between detector models are visible.

We use the reconstructed polarimeter distributions to run a series of pseudo-experiments to estimate the precision with which we can estimate the fraction of positive and negative helicity taus in high invariant-mass tau pairs, produced in each beam polarisation sample. We assume that the helicity fractions of events with invriant mass below 480 GeV are as in the SM, and attempt to measure the polarisation of only those above 480 GeV. We assume that the background distributions are understood exactly. The resulting distributions, normalised to the expected integrated luminosity, are shown in figs 16, 17 for each of the four polarisation combinations (assuming 80/30 beam polarisation) in the two considered tau decay modes.

These templates were used to run a series of pseudo-experiments, which were then fitted to extract the polarisation of taus in high-mass pair events. This procedure was repeated with various levels of "cheating". In the first, we use the "EXACT" form for the polarimeters, including the neutrino momenta, and using the MC truth for 4-momenta. In the "APPROX" case, we use the polarimeter forms given in the appendix. We investigate the effect of event selection, ECAL resolution, and backgrounds. The precision on the determination of this polarisation (the mean of the distribution of parameter fit errors in the ensemble of pseudo-experiments) are shown in tables 3, 4, together with some more technical details and checks of the fits. The main results are shown graphically in Fig. 18.

The two decay modes have rather similar precision, the smaller statistics of the pion mode being compensated by its greater per-event distinguishing power. There is no clear advantage for either of the two detector models. The differences seen in the various measurements, which when seen together do not favour any particular model, are likely due to MC statistics of the fit templates.

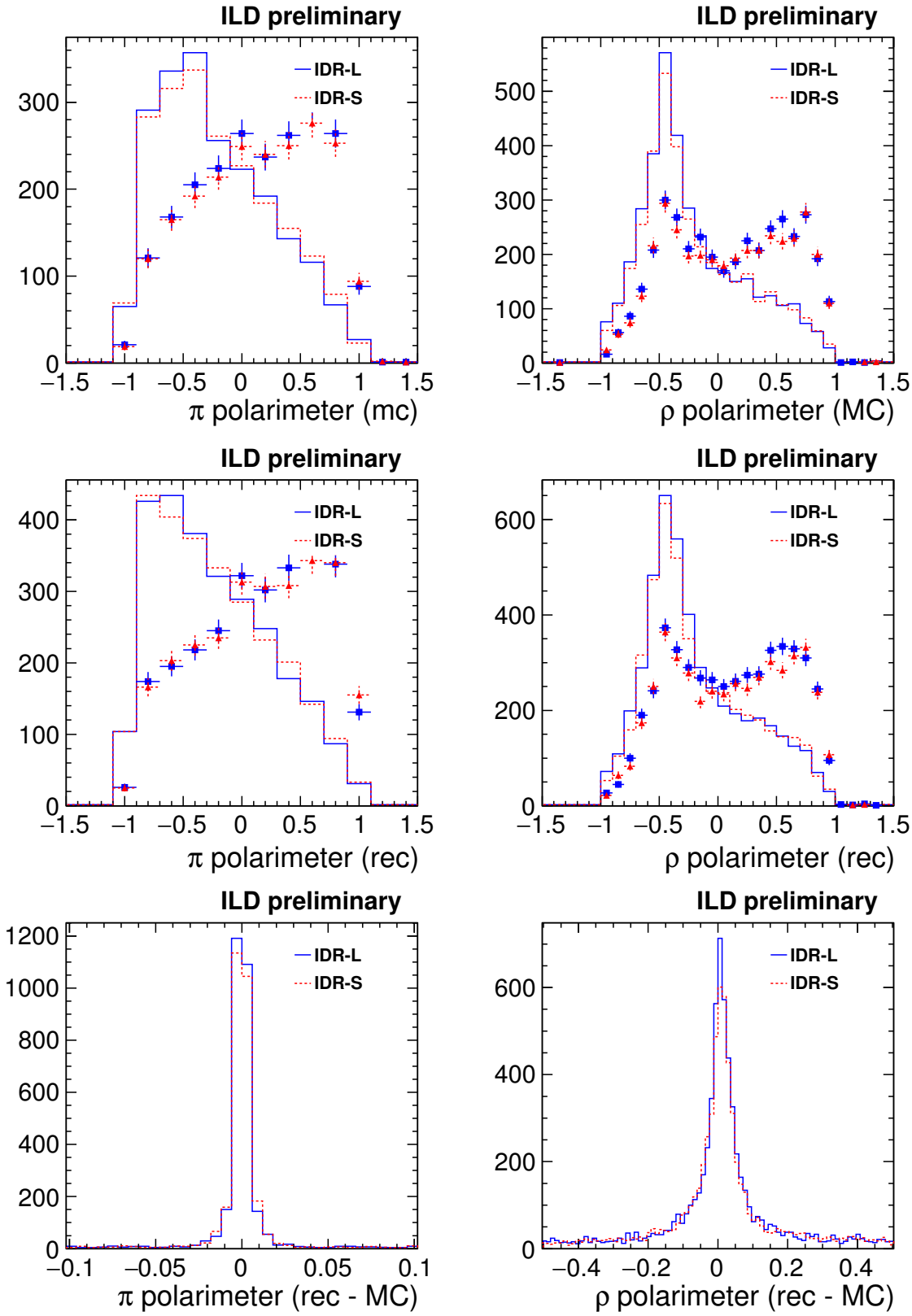

Figure 15: Polarimeters in selected and correctly identified taus. Top: distributions of the true polarimeters for jets in selected signal events: the full line histograms are for 100% eLpR beam polarisation, and the markers with error bars are for 100% eRpL polarisation. Middle: the same for the reconstructed polarimeters. Bottom: the jet-by-jet difference between the reconstructed and true polarimeter values.

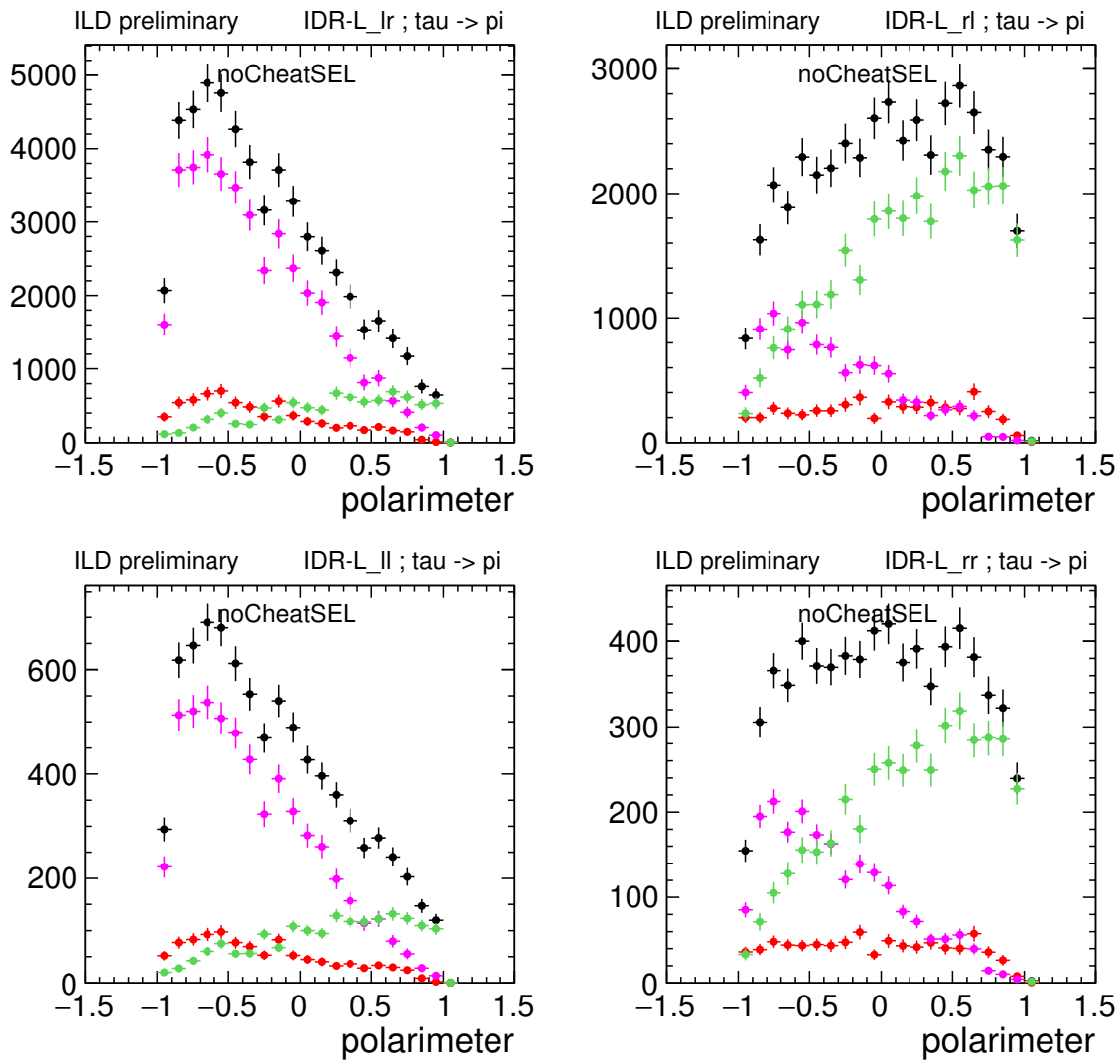

Figure 16: Polarimeter templates for $\tau \to \pi$ decays, scaled to the expected integrated luminosity in the four polarisation scenarios. Black=total, pink=negative hel, green=positive hel, red=background. The signal includes events with invariant tau-tau mass of at least 480 GeV, and at least one hadronic tau decay. The background distribution is dominated by tau-pair events with lower invariant mass, together with a rather small contribution from other 2-f and 4-f events. Error bars are due to finite MC statistics, which were ignored when estimating the measurement precision. IDR-L detector model.

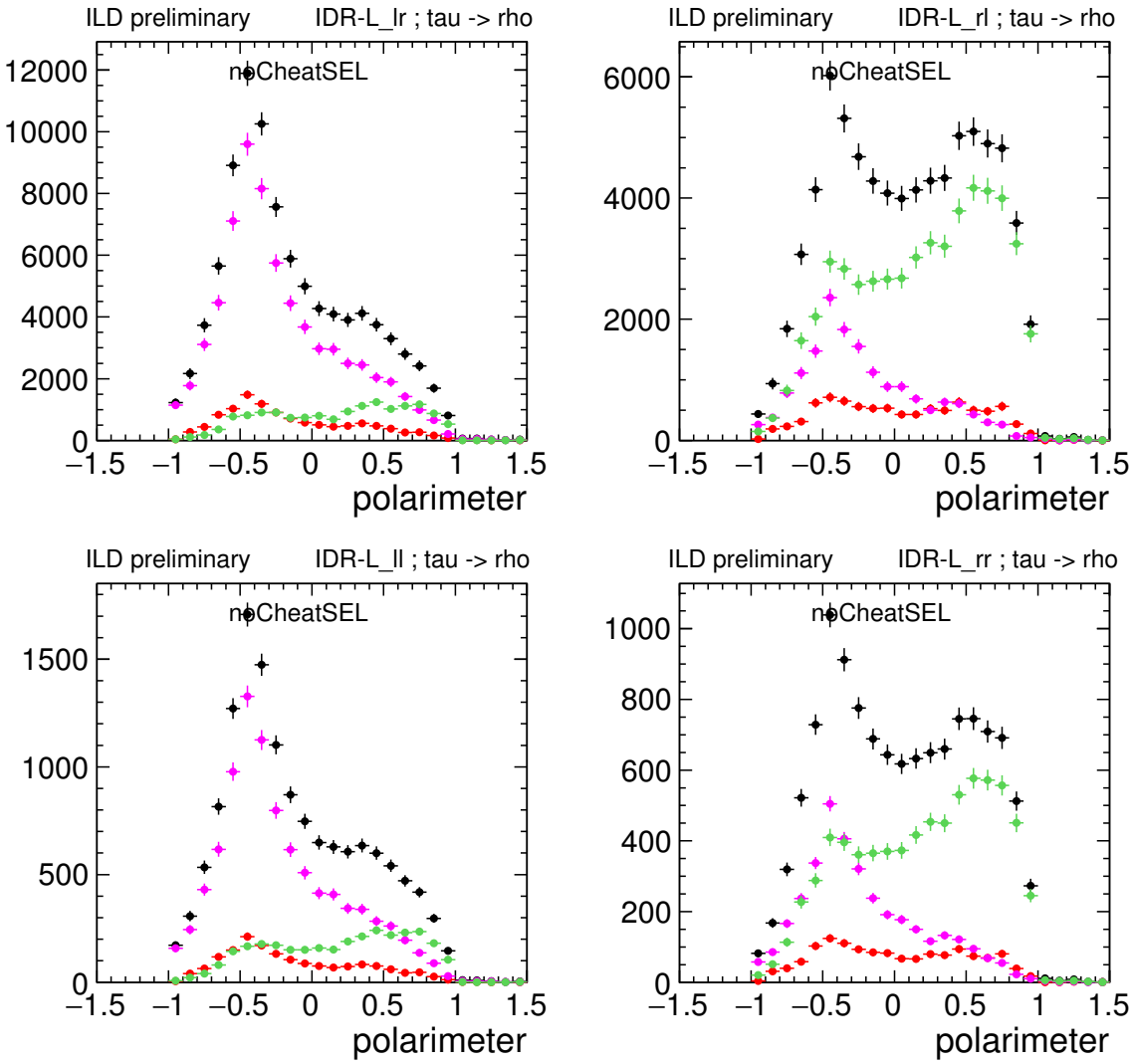

Figure 17: Polarimeter templates for $\tau \to \rho$ decays, scaled to the expected integrated luminosity in the four polarisation scenarios. Black=total, pink=negative hel, green=positive hel, red=background. Error bars are due to finite MC statistics, and are ignored when estimating the measurement precision. IDR-L detector model.

Cheat	EXACT MC		APPROX MC		NONE			
SEL	NO		YES					
BG	NO						YES	
detector			IDR-L	IDR-S	IDR-L	IDR-S	IDR-L	IDR-S
INPUT POL %								
eLpR	−62.1	−62.1	−63.7	−62.4	−64.6	−63.8	−64.6	−63.8
eRpL	52.8	52.8	53.9	53.6	51.3	51.8	51.3	51.8
eLpL	−49.5	−49.5	−50.7	−49.5	−52.1	−51.5	−52.1	−51.5
eRpR	35.5	35.5	36.2	36.2	33.5	33.8	33.5	33.8
NEVENTS								
eLpR	114963	114963	44294	44148	48906	50296	55752	57469
eRpL	96002	96002	36949	36963	39845	40639	45011	46000
eLpL	17240	17240	6642	6622	7314	7516	8333	8580
eRpR	15085	15085	5807	5806	6285	6418	7114	7278
FITTED POL %								
eLpR	-62.1 ± 0.0	-62.1 ± 0.0	-63.7 ± 0.0	-62.3 ± 0.0	-64.6 ± 0.0	-63.8 ± 0.0	-64.6 ± 0.0	-63.8 ± 0.0
eRpL	52.8 ± 0.0	52.8 ± 0.0	53.9 ± 0.0	53.6 ± 0.0	51.3 ± 0.0	51.7 ± 0.0	51.3 ± 0.0	51.8 ± 0.0
eLpL	-49.4 ± 0.0	-49.5 ± 0.0	-50.7 ± 0.0	-49.5 ± 0.0	-52.1 ± 0.0	-51.4 ± 0.0	-52.0 ± 0.0	-51.5 ± 0.0
eRpR	35.5 ± 0.0	35.5 ± 0.0	36.1 ± 0.0	36.2 ± 0.0	33.5 ± 0.0	33.8 ± 0.0	33.4 ± 0.0	33.8 ± 0.0
MEAN FITTED POL Error %								
eLpR	0.46	0.46	0.78	0.80	0.78	0.79	0.82	0.83
eRpL	0.52	0.52	0.90	0.87	1.02	0.98	1.08	1.04
eLpL	1.24	1.25	2.13	2.16	2.15	2.16	2.26	2.28
eRpR	1.39	1.40	2.39	2.34	2.62	2.55	2.79	2.71
PULL MEAN								
eLpR	0.02 ± 0.01	-0.01 ± 0.01	-0.02 ± 0.01	-0.00 ± 0.01	-0.01 ± 0.01	0.01 ± 0.01	0.01 ± 0.01	0.02 ± 0.01
eRpL	-0.01 ± 0.01	0.01 ± 0.01	-0.01 ± 0.01	-0.00 ± 0.01	0.01 ± 0.01	-0.02 ± 0.01	0.00 ± 0.01	0.00 ± 0.01
eLpL	0.01 ± 0.01	-0.01 ± 0.01	-0.00 ± 0.01	0.02 ± 0.01	-0.00 ± 0.01	-0.00 ± 0.01	0.00 ± 0.01	-0.02 ± 0.01
eRpR	-0.01 ± 0.01	-0.00 ± 0.01	-0.00 ± 0.01	0.02 ± 0.01	0.00 ± 0.01	0.01 ± 0.01	-0.02 ± 0.01	-0.00 ± 0.01
PULL WIDTH								
eLpR	1.01 ± 0.01	0.99 ± 0.01	1.00 ± 0.01	1.01 ± 0.01	1.00 ± 0.01	1.00 ± 0.01	1.00 ± 0.01	1.00 ± 0.01
eRpL	1.01 ± 0.01	0.99 ± 0.01	1.00 ± 0.01	1.02 ± 0.01	0.99 ± 0.01	1.00 ± 0.01	1.00 ± 0.01	1.00 ± 0.01
eLpL	1.00 ± 0.01	1.01 ± 0.01	0.99 ± 0.01	1.02 ± 0.01	1.00 ± 0.01	1.00 ± 0.01	0.99 ± 0.01	0.98 ± 0.01
eRpR	1.00 ± 0.01	1.00 ± 0.01	1.00 ± 0.01	0.99 ± 0.01	1.00 ± 0.01	1.01 ± 0.01	0.99 ± 0.01	1.01 ± 0.01

Table 3: pion decay mode, 5k pexps

Cheat	EXACT		APPROX		ECAL		NONE			
evtSel	NO		YES							
BG	NO								YES	
detector			IDR-L	IDR-S	IDR-L	IDR-S	IDR-L	IDR-S	IDR-L	IDR-S
INPUT POL %										
eLpR	−62.9	−61.9	−63.1	−62.8	−63.1	−61.9	−63.5	−61.9	−63.5	−61.9
eRpL	52.7	53.9	52.1	52.7	52.6	52.9	52.5	52.8	52.5	52.8
eLpL	−50.4	−49.0	−50.5	−50.5	−50.4	−49.3	−50.8	−49.5	−50.8	−49.5
eRpR	35.0	36.5	34.6	34.8	35.1	35.5	34.8	35.3	34.8	35.3
NEVENTS										
eLpR	262263	252181	94367	94092	83058	82126	82550	81694	93655	93034
eRpL	215809	211683	78354	76091	68996	67958	68277	67288	77090	76113
eLpL	39266	37839	14142	14061	12448	12303	12366	12232	14024	13921
eRpR	33987	33237	12323	12015	10850	10693	10744	10595	12142	12000
FITTED POL %										
eLpR	-62.9 ± 0.0	-61.9 ± 0.0	-63.1 ± 0.0	-62.8 ± 0.0	-63.2 ± 0.0	-61.9 ± 0.0	-63.5 ± 0.0	-61.9 ± 0.0	-63.5 ± 0.0	-61.9 ± 0.0
eRpL	52.7 ± 0.0	53.9 ± 0.0	52.1 ± 0.0	52.7 ± 0.0	52.6 ± 0.0	52.9 ± 0.0	52.4 ± 0.0	52.8 ± 0.0	52.5 ± 0.0	52.8 ± 0.0
eLpL	-50.4 ± 0.0	-49.0 ± 0.0	-50.5 ± 0.0	-50.4 ± 0.0	-50.4 ± 0.0	-49.4 ± 0.0	-50.8 ± 0.0	-49.5 ± 0.0	-50.8 ± 0.0	-49.5 ± 0.0
eRpR	35.0 ± 0.0	36.5 ± 0.0	34.6 ± 0.0	34.8 ± 0.0	35.1 ± 0.0	35.5 ± 0.0	34.8 ± 0.0	35.3 ± 0.0	34.9 ± 0.0	35.3 ± 0.0
MEAN FITTED POL Error %										
eLpR	0.31	0.40	0.64	0.64	0.70	0.70	0.74	0.73	0.79	0.77
eRpL	0.34	0.49	0.81	0.85	0.91	0.94	0.92	0.97	0.98	1.03
eLpL	0.84	1.07	1.73	1.75	1.88	1.91	2.00	1.97	2.11	2.09
eRpR	0.92	1.25	2.05	2.15	2.28	2.36	2.33	2.43	2.47	2.58
PULL MEAN										
eLpR	-0.00 ± 0.01	-0.02 ± 0.01	0.01 ± 0.01	-0.01 ± 0.01	-0.02 ± 0.01	-0.01 ± 0.01	-0.01 ± 0.01	0.01 ± 0.01	-0.01 ± 0.01	0.00 ± 0.01
eRpL	0.00 ± 0.01	0.01 ± 0.01	0.01 ± 0.01	-0.02 ± 0.01	0.00 ± 0.01	-0.00 ± 0.01	-0.02 ± 0.01	-0.01 ± 0.01	0.01 ± 0.01	0.00 ± 0.01
eLpL	-0.00 ± 0.01	-0.00 ± 0.01	-0.01 ± 0.01	0.02 ± 0.01	-0.01 ± 0.01	-0.04 ± 0.01	0.00 ± 0.01	-0.01 ± 0.01	0.00 ± 0.01	-0.01 ± 0.01
eRpR	0.00 ± 0.01	-0.00 ± 0.01	-0.03 ± 0.01	-0.00 ± 0.01	0.00 ± 0.01	0.01 ± 0.01	-0.02 ± 0.01	0.00 ± 0.01	0.02 ± 0.01	0.00 ± 0.01
PULL WIDTH										
eLpR	1.01 ± 0.01	1.00 ± 0.01	1.02 ± 0.01	1.01 ± 0.01	0.99 ± 0.01	1.01 ± 0.01	1.00 ± 0.01	0.99 ± 0.01	1.01 ± 0.01	1.00 ± 0.01
eRpL	1.01 ± 0.01	0.99 ± 0.01	1.00 ± 0.01	1.01 ± 0.01	0.98 ± 0.01	0.99 ± 0.01	1.01 ± 0.01	1.00 ± 0.01	0.99 ± 0.01	1.01 ± 0.01
eLpL	1.02 ± 0.01	1.02 ± 0.01	1.01 ± 0.01	1.00 ± 0.01	0.99 ± 0.01	1.01 ± 0.01	1.00 ± 0.01	1.00 ± 0.01	1.00 ± 0.01	1.01 ± 0.01
eRpR	0.99 ± 0.01	0.99 ± 0.01	1.00 ± 0.01	1.01 ± 0.01	0.99 ± 0.01	0.98 ± 0.01	1.00 ± 0.01	0.99 ± 0.01	0.99 ± 0.01	1.01 ± 0.01

Table 4: rho decay mode, results of 5k pseudo-experiments.

5.1 Fancy methods which don't (yet) work very well

In the case of single pion decay, the optimal polarimeter is very simple: the ratio of the pion energy to the beam energy (assuming that the taus are exactly back-to-back). In the case of rho decay, full sensitivity to the tau lepton polarisation requires reconstruction of the neutrino momenta. Attempts were made to use and develop such methods, which so far achieved only limited success. We report on them for completeness.

In the case of back-to-back taus of known energy, the neutrino momenta can be estimated by constraining the tau lepton energies (250 GeV), their being back-to-back, and imposing the known tau mass. Zero or two (possibly identical) solutions occur, which correspond to the momentum lying along intersection of 2 cones around the visible tau momenta. It is not clear to me how to choose between these 2 solutions. In events with only pi and rho decays, a good solution was found in only around one third of events.

An alternative method is based on the impact parameter of the charged particles, as described in [2] and used in [3]. We know that the tau must decay somewhere on the charged particle's trajectory. If we know the IP position, we can therefore constrain the tau momentum to lie in the plane defined by the trajectory and the IP. In the events discussed here, the IP cannot be directly measured, since no prompt tracks are produced in the reaction. However, the small ILC interaction region provides a strong constraint in the transverse plane. To estimate the position in z, we simply take the average of the tau jet seeds' z0 track parameters. Better results may come from scanning along z, and finding the "best" solution, or by requiring a multi-prong decay of one of the taus in an event. By assuming a single neutrino per tau decay and imposing the tau mass, we find neutrino momenta which result in positive tau decay lengths and minimise the pT of the tau-tau system. Using this method, again only about a third of events could be reconstructed.

In the future, it would be interesting to combine elements of these two methods, which will hopefully result in a more robust technique for fully reconstructing the tau momentum.

6 Conclusion

Acknowledgments

References

[1] L. Duflot, "Nouvelle méthode de mesure de la polarisation du τ. Application au canal $\tau \to a_1 \nu_\tau$ dans l'expérience ALEPH.," LAL-93-09.

[2] D. Jeans, "Tau lepton reconstruction at collider experiments using impact parameters," Nucl. Instrum. Meth. A **810**, 51 (2016)

[3] D. Jeans and G. W. Wilson, "Measuring the CP state of tau lepton pairs from Higgs decay at the ILC," Phys. Rev. D **98**, no. 1, 013007 (2018)

A Explicit expressions for polarimeters

We here reproduce the expressions given in [1], and used in the present analysis, for polarimeters in $\tau \to \pi$ and $\tau \to \rho$ decays.

A.1 $\tau \to \pi$

The polarimeter ω_π can then be written as

$$\omega_\pi = 2x - 1 \tag{1}$$

where $x = E_\pi / E_\tau$, the ratio of the pion energy to that of the τ (which is assumed to be half the centre-of-mass energy in the present case of di-tau production).

A.2 $\tau \to \rho$

Define Q^2 as the squared invariant mass of the two-pion system, θ as the angle between the direction of the hadronic system and the τ momentum in the τ rest frame, and β as the angle between the directions of the charged pion and the total hadronic momenta, in the hadronic rest frame. The angle ψ, between the τ and (minus) the hadronic momentum, in the hadronic rest frame, which can in the case of di-tau production at known centre-of-mass energy, be calculated as

$$\cos\psi = \frac{x(m_\tau^2 + Q^2) - 2Q^2}{(m_\tau^2 - Q^2)\sqrt{x^2 - 4Q^2/s}} \tag{2}$$

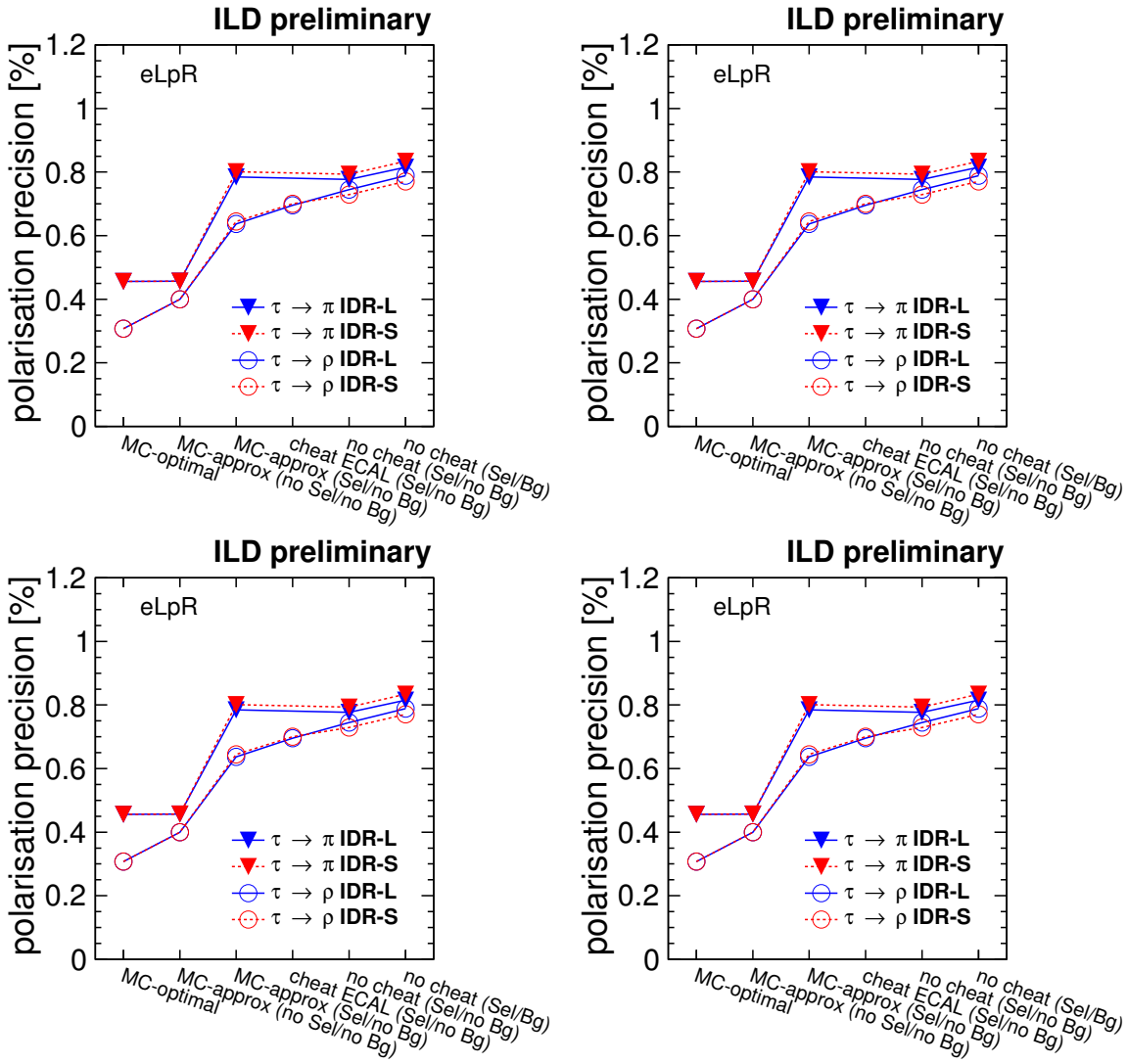

Figure 18: Polarimeter estimation for different levels of cheating, different detector models, and different polarisation sets.

where $x - 2E_h/\sqrt{s}$, with E_h being the energy of the hadronic system in the lab frame and s the squared centre-of-mass energy.

The polarimeter ω_ρ can then be written as

$$\omega_\rho = \frac{(-2 + \frac{m_\tau^2}{Q^2} + 2(1 + \frac{m_\tau^2}{Q^2})\frac{3\cos\psi - 1}{2}\frac{3\cos^2\beta - 1}{2})\cos\theta + 3\sqrt{\frac{m_\tau^2}{Q^2}}\frac{3\cos^2\beta - 1}{2}\sin 2\psi \sin\theta}{2 + \frac{m_\tau^2}{Q^2} - 2(1 - \frac{m_\tau^2}{Q^2})\frac{3\cos\psi - 1}{2}\frac{3\cos^2\beta - 1}{2}} \tag{3}$$

(corresponding to eq. 3.11 of [1]).